Application of robust anti-windup techniques to dynamically substructured systems

Guang Li, *Member, IEEE,* Guido Herrmann, *Senior Member, IEEE,* David P. Stoten, Jiaying Tu and Matthew C. Turner

Abstract—Dynamically substructured systems (DSS) play an important role in modern testing methods. DSS enables full-size critical components of a complete system to be tested physically in real-time, whilst the remaining parts of the system run in parallel as a real-time simulation. The performance of DSS testing is influenced by the synchronization of the physical and numerical substructures, which necessitates the design of a DSS controller. Since the testing signal is known and can be assumed to be a perfectly measured disturbance, the DSS control can be viewed as a regulation control problem with measured disturbance attenuation. A potential problem with DSS control arises from actuator saturation, which can be encountered in DSS transfer systems and can significantly influence the testing accuracy. This paper demonstrates the application of a novel robust disturbance rejection anti-windup (AW) technique, to cope with the actuator saturation problem in DSS. Implementation results from a hydraulically-actuated DSS test rig confirm the advantage of using this novel approach over some other existing AW approaches. Furthermore, some specific practical issues are discussed for the AW compensator design, such as the tuning of parameters.

Index Terms—Keywords: Anti-windup compensation, Dynamic testing, Dynamically substructured systems, Servohydraulically-actuated systems.

I. INTRODUCTION

A. A brief introduction to dynamically substructured systems and their control

THE concept of dynamically substructured systems (DSS) is to use a mixed system containing physical components (called physical substructures) and numerical components (called numerical substructures), to replace the original (or emulated system) during dynamic testing. This idea can overcome drawbacks involved with purely numerical or purely physical testing. For example, some physical components may contain significant uncertainties and nonlinearities, so that replacing them by an estimated numerical model may greatly influence the testing results. On the other hand, using some physical components in a testing procedure may be either unnecessary or unrealistic (e.g., the inclusion of a full-size dam or bridge within a laboratory environment). See [1], [2] for a detailed

G. Li is with School of Engineering, Computing and Mathematics, University of Exeter, Harrison Building, Streatham Campus, North Park Road, Exeter, EX4 4QF, UK. g.li@exeter.ac.uk

G. Herrmann, D. P. Stoten and J. Tu are with the Advanced Control and Test Laboratory (ACTLab), Department of Mechanical Engineering, The University of Bristol, Queens Building, University Walk, Bristol, BS8 1TR, UK. {g.herrmann, d.p.stoten, jiaying.tu}@bristol.ac.uk

M. C. Turner is with the Control and Instrumentation Research Group, Department of Engineering, University of Leicester, University Road, Leicester, LE1 7RH, UK. mct6@le.ac.uk

discussion on the advantage of using DSS. The uses of the DSS concept can be found in areas such as automotive [3], aerospace [4], civil engineering [5]–[8] and robotics [9].

DSS is distinguishable from the hardware-in-the-loop (HIL) method, which is used traditionally to test the performance of a controller, with a hardware interface to an embedded numerical plant (see, e.g. [10], [11]). However, in more recent developments, the HIL approach has some common features with the DSS methodology; for example, see [12]–[14]. The distinguishing feature of DSS is to produce a composite system involving both numerical and physical testing components, which must be synchronized at their interfaces in order to create a similar testing environment to the original emulated system.

The employment of DSS in the civil engineering area has been significant [5]–[8], [15] and will serve in this section as an introductory example for a typical DSS-application, i.e. the testing of a building during an earthquake. Instead of testing the whole building on a shaking table (which is usually not realistic), only the upper part of the building is tested physically, while the remaining lower part is simulated simultaneously in a computer [5]. The objective is to make the responses from this substructured building as close as possible to the original whole building when subject to the same testing signal. In the DSS-case, the test signal acts on the lower, simulated part of the building.

Often, the schematic representation of a DSS can be depicted as in Fig. 1 [1]. This DSS contains one numerical substructure Σ_N and one physical substructure Σ_P, although the total number of numerical substructures and physical substructures are not necessarily limited to one of each type. The physical substructure typically consists of a number of interconnected components: actuator(s), a test-frame structure, a test specimen, an inner-loop controller, and sensor(s). The testing signal d represents an external excitation input to the emulated system, Σ_E, typically an environmental disturbance (e.g. seismic, air turbulence, road inputs). The displacements $\{z_N, z_P\}$ and forces $\{f_N, f_P\}$ are the response signals of Σ_N and Σ_P at their interfaces; hence, we call them interface signals. The interface signals are separated into two sets: one set is chosen as the constraint signals $\{f_N, f_P\}$ and the other set as the synchronization signals $\{z_N, z_P\}$. This choice may change in different situations. When measurement noise is ignored, the constraint signals satisfy $f_N = f_P$. The purpose of the control signal u is to ensure that the difference between z_N and z_P, defined as the DSS error $e := z_N - z_P$, is kept as near to zero as possible. It can be shown that when e is small, the DSS responses will be closer to those of the emulated system. This is called DSS *synchronization*, so that the DSS
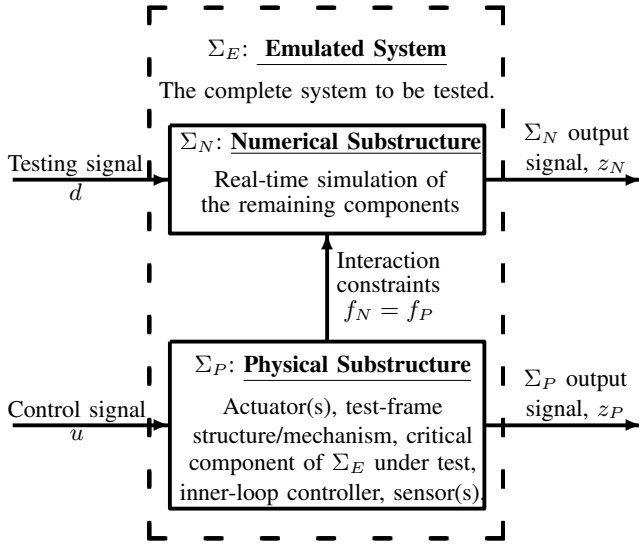
Fig. 1: An illustration of dynamically substructured system [1].

error is driven towards zero by a control signal u.

This synchronization requires a DSS controller, which must also negate the dynamical effects of additional actuators in the physical substructures. To facilitate the DSS controller design, we use the DSS framework illustrated in Fig. 2, which is generalized from Fig. 1 and modified from the original in [1], by extracting out the transfer system (i.e. the actuator system), represented by G_A, to signify its role in the DSS:

$$z_N = G_d d - G_I G_A u \tag{1a}$$
$$z_P = G_A u \tag{1b}$$

Here, z_N and z_P are DSS output signals; the control signal u is provided by a DSS controller; G_d contains the components which are subject to the testing signal d; G_I represents the interaction between G_A and the remaining system. G_I and G_d may consist of both numerical and/or physical components, and the constraint signals are contained in G_I. Note that a specific investigation of the internal structures and signals can help design more sophisticated controllers (e.g. by taking into account measurement noise from the physical and numerical interface and locating the origin of the uncertainties in the physical substructure). However, in this paper, our emphasis is mainly on the design of a robustly performing AW compensator imposed on a pre-designed linear controller. It is generally not very efficient for H_∞ and LMI based designs to consider each specific internal structure and signal explicitly, if there is no specific issue. Hence, the DSS controller designs are simplified by assuming the uncertainties can be lumped into uncertainty blocks. (Later practical results will demonstrate this assumption to be correct.) The DSS control described above can be cast into a regulation problem, with measured disturbance rejection, since the testing (excitation) signal d will always be a measurable disturbance.
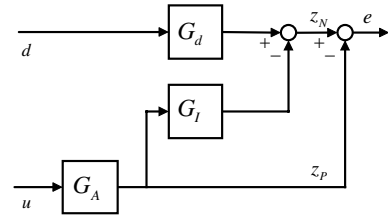

Fig. 2: The DSS framework [1]

B. Coping with actuator saturation problem in DSS testing using anti-windup compensation

One of the main issues with DSS control is associated with the performance of the actuators. Much of the work in DSS control is about how to overcome the limiting dynamic characterisics of actuators, e.g. phase/time delays [16], [17] and hard limits [13]–[15], etc. This paper addresses how to use anti-windup (AW) compensation techniques to cope with actuator saturation problem. Although every effort for appropriate actuator selection should be made at the design stage, there are still some important issues for consideration:

1) Hard input constraints should be enforced on actuators to prevent them from triggering safety limits, for safety reasons.
2) In order to achieve the best synchronization during DSS testing, the actuators are often expected to run at their full capabilities. This is because it is often the case that driving actuators into saturation can result in better performance than using cautious controllers that remain inside the saturation limits.
3) Since the cost of an actuator can increase dramatically with performance, it is reasonable to use a less expensive actuator to achieve a satisfactory performance.
4) In some cases, a sufficiently powerful actuator may not be available (e.g. structure testing in civil engineering). In this case, it is not possible to use an actuator without avoiding saturation.

Potential control strategies for coping with actuator saturation include model predictive control (MPC) and anti-windup (AW) compensation. The MPC strategy has been successfully implemented on a hydraulically-actuated test rig developed at the University of Bristol, with sampling rates up to 1kHz [18]. Although such sampling rates are applicable under the current testing environment, problems may occur when the testing of DSS systems requires a higher sampling rate, or the on-line computational burden of MPC increases with model order and prediction horizon length. For this reason, we propose to use AW compensation as an alternative strategy to reduce the online computational requirements. Various AW approaches have been extensively studied in theory and practice, e.g. [19]–[26]. The framework proposed by Weston and Postlethwaite in [27] has found application in a number of different areas, e.g. see [28], [29]. Following the framework in [27], an AW approach for the disturbance rejection problem is proposed in [30], where numerical results show performance improvement over alternative approaches. In a recent work [31], we have further modified this AW approach for improving its robust

TABLE I: Notation list for the QM system – Variables

Notation	Description
y_1, y_2	Front/rear wheel displacements.
y_b	Body center of mass displacement.
θ	Pitch angle of the body.
y_{b31}, y_{b32}	Front/rear ends of body displacements.
y_{31}, y_{32}	Front/rear suspension base displacements.
u_1, u_2	Inputs of the front/rear suspension actuators.
f_1, f_2	Interaction forces.
d_1, d_2	Disturbances on the front/rear wheels.

TABLE II: Notation list for the QM system – Parameters

Notation	Description	Values
	Quasi-motorcycle body:	
m_3	Mass	229kg
J	Moment of inertia	62.7kgm^2
L	Body length	1.60m
L_1, L_2	Lengths from front/rear end to mass center	0.800m, 0.800m
	Front/rear suspension:	
k_{31}, k_{32}	Stiffness	34.8kN/m, 39.5kN/m
c_{31}, c_{32}	Damping	717Ns/m, 970Ns/m
	Front/rear wheels:	
m_1, m_2	Mass	12.3kg, 15.7kg
k_1, k_2	Stiffness	384kN/m, 409kN/m
c_1, c_2	Damping	700Ns/m, 816Ns/m

performance by incorporating an additive uncertainty into the synthesis procedure.

In this paper, we implement this AW approach, together with other existing AW approaches for comparison purposes, on a servohydraulically-actuated quasi-motorcycle test rig, developed at the University of Bristol for real-time testing of DSS configurations. The issues in the design and implementation of the AW compensators in real-time applications have also been addressed. Hence the main contributions of this paper are to demonstrate the efficacy of the novel AW compensation approach in [31], and also to provide a systematic procedure of AW compensator design for DSS systems.

The results of implementing three AW approaches are presented: 1) the robust disturbance rejection AW (DRAW) approach modified from [30]; 2) the robust AW (RAW) approach of [32], [33]; 3) the internal model control (IMC) based AW (IMC AW) approach [19]. Both DRAW and RAW are based on the framework of Weston and Postlethwaite in [27], and subsume IMC AW as a special case. RAW is mainly for regulation problems, whilst DRAW is for measured disturbance rejection problems, which can be specifically tailored for coping with DSS saturation. DRAW extends ideas from [30] to include robust performance for additive uncertainties.

The paper is organized as follows. Section II introduces the test rig and its two DSS formulations. Section III presents the AW approaches. Section IV presents H_∞ controller designs, the tuning of AW compensators and the implementation results for the two DSS developed in section II. Section V concludes the paper.

II. SUBSTRUCTURING FOR A QUASI-MOTORCYCLE (QM) HYDRAULICALLY-ACTUATED SYSTEM

A. The test rig and its substructured form

We consider a quasi-motorcycle (QM) hydraulically-actuated system, developed at the University of Bristol; see Fig. 3 for a photograph of the rig and Fig. 4 for its schematic representation. The test rig is composed of three subsystems, the first of which is a rigid vehicle body, with an evenly distributed mass of 229kg, and two suspension struts. The latter are connected to the vehicle body at one end and to two 25kN hydraulic actuators (via swing arms) at the other end. The second and third subsystems consist of two separate 25kN hydraulic actuators, attached to the hubs of the front and rear wheels/tires. Each hydraulic actuator has a built-in linear variable differential transformer (LVDT) for the measurement of displacement and also a load cell for the measurement of force. For test purposes, we can select each subsystem either

as a numerical or a physical element. Hence, we can derive different DSS for this test rig, which are classified according to the type of forces at the interfaces between the subsystems [34]. In this paper, we only focus on two scenarios. In scenario 1, the QM body with the two suspension struts constitute the physical substructure, while the front and rear wheels form the numerical substructure. We call this a *single mode* substructure (SiM) since only one type of force, i.e. inertial terms, occur in the physical substructure. In scenario 2, the two wheels are chosen as the physical substructure and the body with two suspension struts as the numerical substructure. We call this a *multi mode* substructure (MuM), since two substructures with the same type of loading (reaction forces) are present in the physical substructure. The interface variables are the displacements and the forces at the attachment points of the wheel hubs and the ends of the swing arms and they are represented respectively as $\{y_{31}, y_{32}\}$, $\{y_1, y_2\}$, $\{f_{31}, f_{32}\}$ and $\{f_1, f_2\}$.

B. Synthesis of the DSS for the test rig

The dynamic equations of the quasi-motorcycle system can be found in [18], [34] (see Fig. 4); the linearized equations of motion, in the Laplace domain, are summarized as follows:

$$y_1 = G_{yd1}d_1 - G_{yf1}f_1 \tag{2}$$

$$y_2 = G_{yd2}d_2 - G_{yf2}f_2 \tag{3}$$

$$f_{31} = P_2 s^2 y_{b31} + P_3 s^2 y_{b32} \tag{4}$$

$$f_{32} = P_3 s^2 y_{b31} + P_1 s^2 y_{b32} \tag{5}$$

$$y_{b31} = G_{31}y_{31} \tag{6}$$

$$y_{b32} = G_{32}y_{32} \tag{7}$$

with

$$G_{yd1} = \frac{c_1 s + k_1}{m_1 s^2 + c_1 s + k_1} \qquad G_{yd2} = \frac{c_2 s + k_2}{m_2 s^2 + c_2 s + k_2}$$

$$G_{yf1} = \frac{1}{m_1 s^2 + c_1 s + k_1} \qquad G_{yf2} = \frac{1}{m_2 s^2 + c_2 s + k_2}$$

$$G_{31} = \frac{c_{31} s + k_{31}}{m_{31} s^2 + c_{31} s + k_{31}} \qquad G_{32} = \frac{c_{32} s + k_{32}}{m_{32} s^2 + c_{32} s + k_{32}}$$

and $P_1 = \frac{m_3 L_{31}^2}{L_3^2} + \frac{J_3}{L_3^2}$, $P_2 = \frac{m_3 L_{32}^2}{L_3^2} + \frac{J_3}{L_3^2}$ and $P_3 = \frac{m_3 L_{31} L_{32}}{L_3^2} - \frac{J_3}{L_3^2}$. Here equations (2) and (3) represent the dynamics of the front and rear wheels; equations (6) and (7)
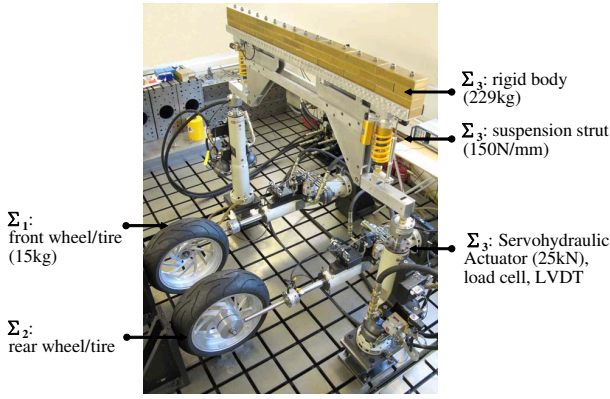
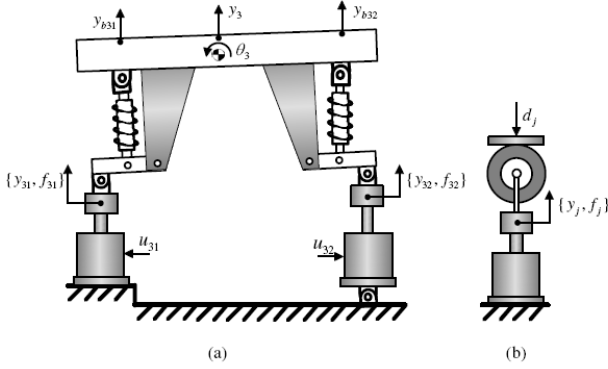Fig. 3: Photograph of the quasi motorcycle test rig

Fig. 4: A schematic representation of the quasi motorcycle test rig: (a) the vehicle body with two suspension struts and two swing arms; (b) the hub and wheels with $j = 1$ for the front and $j = 2$ for the rear.

represent the dynamics of the front and rear suspension struts; and equations (4) and (5) reflect the dynamical interaction between the front and rear parts of the vehicle through the vehicle body. All the variables and parameters, with their nominal values, are listed in Tables I and II.

Based on these relations, the SiM and MuM can be converted into the DSS framework of Fig. 2, as shown in the following two subsections.

1) Scenario 1 – SiM: Suppose the forces $\{f_{31}, f_{32}\}$ are chosen as the constraint signals, while the displacements $\{y_{31}, y_{32}\}$ are the synchronizing signals, which are generated by the action of the inner-loop controlled actuators $y_{31} = G_{Ay1}u_{31}$ and $y_{32} = G_{Ay2}u_{32}$ with the displacement output transfer functions identified as $G_{Ay1} = G_{Ay2} = \frac{43.6}{s+37.6}$.

By manipulation of equations (2)-(7), the SiM can be represented by the DSS framework of (1), with $z_N = [y_1, y_2]^T$, $z_P = [y_{31}, y_{32}]^T$, $d = [d_1, d_2]^T$, $u = [u_{31}, u_{32}]^T$, $G_d = \text{diag}(G_{yd1}, G_{yd2})$, $G_A = \text{diag}(G_{Ay1}, G_{Ay2})$ and

$$G_I = \begin{bmatrix} G_{yf1}P_2 s^2 G_{31} & G_{yf1}P_3 s^2 G_{32} \\ G_{yf2}P_3 s^2 G_{31} & G_{yf2}P_1 s^2 G_{32} \end{bmatrix}.$$

2) Scenario 2 – MuM: Suppose the displacements $\{y_{31}, y_{32}\}$ are chosen as the constraint signals, while the forces $\{f_{31}, f_{32}\}$ are the synchronizing signals, which are generated by the action of the inner-loop controlled actuators

$f_{31} = G_{Af1}u_1$ and $f_{32} = G_{Af2}u_2$ with the force output transfer functions identified as $G_{Af1} = G_{Af2} = \frac{13.5}{s+12.9}$.

Manipulation of equations (2)-(7) enables the MuM to be represented by the DSS framework of (1), with $z_N = [f_{31}, f_{32}]^T$, $z_P = [f_1, f_2]^T$, and

$$G_d = \begin{bmatrix} P_2 s^2 G_{31} G_{yd1} & P_3 s^2 G_{32} G_{yd2} \\ P_3 s^2 G_{31} G_{yd1} & P_1 s^2 G_{32} G_{yd2} \end{bmatrix},$$

$$G_I = \begin{bmatrix} P_2 s^2 G_{31} G_{yf1} & P_3 s^2 G_{32} G_{yf2} \\ P_3 s^2 G_{31} G_{yf1} & P_1 s^2 G_{32} G_{yf2} \end{bmatrix},$$

$$G_A = \text{diag}(G_{Af1}, G_{Af2}).$$

III. THE ANTI-WINDUP (AW) APPROACHES

The AW scheme to be employed is inspired by the framework proposed in [27], also shown in Fig. 5, but with the introduction of a novel concept for robustness in AW compensation (see [31]). The transfer functions for the plant and controller are

$$\mathcal{P}(s) = \begin{bmatrix} \mathcal{P}_w(s) & \mathcal{P}_u(s) \end{bmatrix} \quad \mathcal{K}(s) = \begin{bmatrix} \mathcal{K}_w(s) & \mathcal{K}_y(s) \end{bmatrix} \quad (8)$$

where all the uncertainties from $\hat{u}$ to y in Fig. 5 are assumed to be lumped into an additive uncertainty, $\Delta(s)$, so that the dynamics from u to y is $\mathcal{P}_u(s) + \Delta(s)$. Note that we assume an additive uncertainty in the plant; this assumption is general enough and is also common practice for robust controller design (see e.g. [32]), since an additive uncertainty can be equivalently represented by other forms of uncertainties, e.g. a multiplicative uncertainty.

The DSS shown in Fig. 2 can then be cast into this framework by setting $\mathcal{P}_u = -(G_I + I)G_A$ and $\mathcal{P}_w = G_d$. We assume a state space realization of $\mathcal{P}_u$ is (A_p, B_p, C_p, D_p).

The AW compensator is given by

$$\begin{bmatrix} \Theta_1(s) \\ \Theta_2(s) \end{bmatrix} \sim \left[\begin{array}{c|c} A_p + B_pF & B_pE \\ \hline F & E - I \\ C_p + D_pF & D_pE \end{array} \right] \quad (9)$$

The system conditioning is achieved by designing F and E.

In the following we concisely present three AW compensation techniques, which can be used to cope with the DSS actuation problem.

A. Disturbance rejection AW (DRAW) with guaranteed robust performance

In order to introduce robustness in the AW compensation design, we modify the approach in [30] by augmenting the DSS testing signal d so that $\tilde{d} = \begin{bmatrix} d^T, d_d^T \end{bmatrix}^T$, where d_d has the same dimension as the plant output y. $\mathcal{K}_w$ is replaced by $\begin{bmatrix} \mathcal{K}_w & w_dI \end{bmatrix}$ and $\mathcal{P}_w$ by $\begin{bmatrix} \mathcal{P}_w & 0 \end{bmatrix}$, where the scalar $w_d > 0$. In this case, we have

$$\mathcal{P}_{\tilde{d}} = (I - \mathcal{K}_y\mathcal{P}_u)^{-1} \left(\begin{bmatrix} \mathcal{K}_w & w_dI \end{bmatrix} + \mathcal{K}_y \begin{bmatrix} \mathcal{P}_w & 0 \end{bmatrix} \right)$$
$$\sim (A_{\tilde{d}}, B_{\tilde{d}}, C_{\tilde{d}}, D_{\tilde{d}}) \quad (10)$$

An AW compensator can be synthesized by minimizing the L_2 gain of

$$\frac{1}{\gamma_d} \left\| \begin{array}{c} W_y^{\frac{1}{2}} y_d \\ W_r^{\frac{1}{2}} u \end{array} \right\|^2 - \gamma_d \|\tilde{d}\|^2 \leq 0 \quad (11)$$

Let $\|\mathcal{T}\|_\infty$ denote the induced L_2 norm of $\mathcal{T}$. In contrast to [30], we minimize not only the induced L_2 gain $\|\mathcal{T}_{y_d}\|_\infty$, where $\mathcal{T}_{y_d} : \tilde{d} \mapsto y_d$, but also the L_2 gain $\|\mathcal{T}_u\|_\infty$, where $\mathcal{T}_u : \tilde{d} \mapsto u$, to achieve robustness and performance. A minimal $\|\mathcal{T}_u\|_\infty$ guarantees robustness to additive uncertainty, while a small $\|\mathcal{T}_{y_d}\|_\infty$ guarantees performance. In (11), the weights W_y and W_r are included to achieve a trade-off between robustness and performance.

Note that the L_2 gain minimization of the mapping $\mathcal{T}_u$ reduces the input u to the nonlinear saturation operator, and hence it directly prevents saturation. By defining the operators $\mathcal{T}_{\hat{u}} : \tilde{d} \mapsto \hat{u}$, $\mathcal{T}_{\text{sat}} : u \mapsto \hat{u}$ in Fig. 5, we have $\|\mathcal{T}_{\hat{u}}\|_\infty = \|\mathcal{T}_{\text{sat}}\mathcal{T}_u\|_\infty \leq \|\mathcal{T}_{\text{sat}}\|_\infty \|\mathcal{T}_u\|_\infty = \|\mathcal{T}_u\|_\infty$, since $\|\mathcal{T}_{\text{sat}}\|_\infty = 1$. This means the minimization of $\|\mathcal{T}_u\|_\infty$ implies the minimization of $\|\mathcal{T}_{\hat{u}}\|_\infty$, which contributes to the reduction of the L_2 gains in the loops from $\tilde{d}$ to y_d and from d to $\hat{u}$. Hence, using the argument of the small gain theorem, we can remark that the inclusion of the minimization of $\|\mathcal{T}_u\|_\infty$ ensures robustness to additive plant uncertainty (see Fig. 5).

The theoretical detail can be found in [31]. Here we just give the synthesis procedure:

Procedure 1 (DRAW compensator synthesis):

1) Given the matrix variable $P = P^T > 0$, solve $\gamma_d^* := \min \gamma_d > 0$ subject to LMIs (12) and (13) to yield P^* and γ_d^*.

$$\begin{bmatrix} PA_o + A_o^T P + PW_A + W_A^T P & W_C + PW_B \\ W_C^T + W_B^T P & W_D \end{bmatrix} < 0 \quad (12)$$

with $A_o = \begin{bmatrix} A_p & 0 \\ 0 & A_{\tilde{d}} \end{bmatrix}$,

$$W_A = \begin{bmatrix} 0 & B_p C_{\tilde{d}} \\ 0 & 0 \end{bmatrix}$$

$$W_B = \begin{bmatrix} B_p D_{\tilde{d}} & 0 & -B_p \\ B_{\tilde{d}} & 0 & 0 \end{bmatrix}$$

$$W_C = \begin{bmatrix} 0 & C_p^T & 0 \\ 0 & C_{\tilde{d}}^T D_p^T & 0 \end{bmatrix}$$

$$W_D = \begin{bmatrix} -\gamma_d I_{n_w} & D_{\tilde{d}}^T D_p^T & 0 \\ D_p D_{\tilde{d}} & -\gamma_d I_{n_y} W_y^{-1} & -D_p \\ 0 & -D_p^T & -\Gamma \end{bmatrix}$$

and

$$\begin{bmatrix} A_{\tilde{d}}^T P_{22} + P_{22} A_{\tilde{d}} & P_{22} B_{\tilde{d}} & C_{\tilde{d}}^T \\ B_{\tilde{d}}^T P_{22} & -\gamma_d I_{n_w} & D_{\tilde{d}}^T \\ C_{\tilde{d}} & D_d & -\gamma_d W_r^{-1} \end{bmatrix} < 0 \quad (13)$$

with $\gamma_d > 0$ and diagonal matrix $\Gamma = \text{diag}(\gamma_1, \ldots, \gamma_{n_u}) > 0$. Here, P is a symmetric positive definite matrix with a structure

$$P := \begin{bmatrix} P_{11} & P_{12} \\ P_{12}^T & P_{22} \end{bmatrix} \in \mathbb{R}^{n_p + n_d} \quad (14)$$

2) Substituting P^* and γ_d^* with some chosen diagonal positive definite W, solve the LMI:
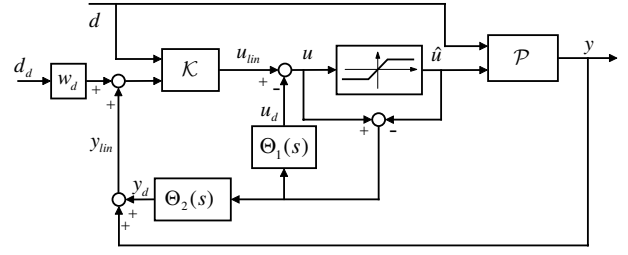
$$\Psi + H^T \Lambda G + G^T \Lambda^T H < 0 \quad (15)$$

Fig. 5: Anti-windup scheme

for Λ, with $\Lambda := \begin{bmatrix} F & E \end{bmatrix}$ and

$$\Psi = \begin{bmatrix} A_o^T P + P A_o & P B_o + C_{do}^T \tilde{W} & C_{po}^T \\ B_o^T P + \tilde{W} C_{do} & \tilde{W} D_{do} + D_{do}^T \tilde{W} - \gamma_d \tilde{I}_{n_w} & 0 \\ C_{po} & 0 & -\gamma_d I_{n_y} \end{bmatrix},$$

$$H = \begin{bmatrix} B_p^T & 0 & | & -I_{n_u} & 0 & | & D_p^T \end{bmatrix} \text{diag}(P, \tilde{W}, I),$$

$$G = \begin{bmatrix} I_{n_p} & 0 & | & 0 & 0_{n_p \times n_w} & | & 0 \\ 0 & 0 & | & I_{n_u} & 0 & | & 0 \end{bmatrix}, \tilde{W} = \begin{bmatrix} W & 0 \\ 0 & I_{n_w} \end{bmatrix}.$$

B. Two other existing AW approaches

For comparison, we also implemented two other AW compensators designed by the robust AW (RAW) approach in [32] and the IMC AW approach [19]. We now present these two approaches for completeness.

1) The RAW approach of [32]: In (9), by assuming $E = I$, we have the framework used to develop the RAW approach in [32]. This approach achieves a tradeoff between performance and robustness, by minimizing the L_2 gain:

$$\frac{1}{\gamma} \left\| \begin{array}{c} W_y^{\frac{1}{2}} y_d \\ W_r^{\frac{1}{2}} z_\Delta \end{array} \right\|^2 - \gamma \|u_{\text{lin}}\|^2 \leq 0 \quad (16)$$

which is composed of a weighted combination of two mappings $\mathcal{T}_p : u_{\text{lin}} \mapsto y_d$ representing the performance and $\mathcal{T}_r : u_{\text{lin}} \mapsto z_\Delta$ representing the robust stability, with W_y and W_r as the corresponding weights. This approach leads to the LMI (23) in [32]:

$$\begin{bmatrix} M_{11} & M_{12} & 0 & M_{14} & L^T \\ \star & -2U & I_{n_u} & U D_p^T & U \\ \star & \star & -\gamma I_{n_u} & 0 & -I \\ \star & \star & \star & -\gamma W_y^{-1} & 0 \\ \star & \star & \star & \star & -\gamma W_r^{-1} \end{bmatrix} < 0 \quad (17)$$

with $M_{11} = A_p Q + Q A_p^T + B_p L + L^T B_p^T$, $M_{12} = B_p U - L^T$, $M_{14} = Q C_p^T + L^T D_p^T$, $Q = Q^T > 0$, $L = FQ$, diagonal matrix $U > 0$ and scalar $\gamma > 0$. A beneficial by-product of involving the extra map $\mathcal{T}_r$ in the minimization is the removal of fast poles of the compensator.

2) IMC AW approach [19]: It is noted that the IMC AW in [19] is subsumed within the AW framework of [32] when we set $F = 0$ and $E = I$ in (9).

C. Remarks on AW tuning in real-time implementations

Some remarks on AW tuning in real-time implementations are given below:

Remark 1: For the DRAW approach and the RAW approach of [32], w_d, W_y and W_r can be used as the tuning parameters to achieve a tradeoff between the performance and robustness, together with the removal of fast poles.

Remark 2: For the DRAW approach and the RAW approach of [32], to achieve better performance over a given frequency range, the transfer function $\mathcal{P}_u$ can be modified by including a filter W_{fy}, so that $\mathcal{P}_u$ is replaced by $W_{fy}\mathcal{P}_u$ when synthesizing the AW compensator.

Remark 3: For the DRAW approach, a filter W_{fd} can also be included to modify $\mathcal{P}_d$, as $\mathcal{K}_{w_{new}} := \mathcal{K}_w W_{fd}$ and $\mathcal{P}_{w_{new}} := \mathcal{P}_w W_{fd}$. A proper choice of W_{fd} can further improve the performance.

When using the AW compensator designed by the DRAW approach, an algebraic loop may arise in the AW framework due to $E \neq I$. Note that the LMIs of (15) guarantee that the algebraic loop has a solution which is unique [35]. Hence, it is now possible to resolve an algebraic loop for a strictly diagonally dominant matrix $(E^{-1}\text{diag}(\bar{u}))$ with $\bar{u}$ as the deadzone limit, using the method proposed in [30]. We present the main steps for resolving an algebraic loop with two constrained signals.

Procedure 2 (Resolving an algebraic loop for two signals): Define the deadzone nonlinearity as

$$\text{dz}_i(u_i) = \begin{cases} u_i + \bar{u}_i, & \text{if } u_i \leq -\bar{u}_i \\ 0, & \text{if } -\bar{u}_i \leq u_i \leq \bar{u}_i \\ u_i - \bar{u}_i, & \text{if } u_i \geq \bar{u}_i \end{cases} \quad (18)$$

where $\bar{u}_i$ with $i = 1, 2$ represent the deadzone limits.

Suppose $E = \left[\begin{smallmatrix} e_{11} & e_{12} \\ e_{21} & e_{22} \end{smallmatrix}\right]$. For a given $\hat{u} = [\hat{u}_1 \ \hat{u}_2]^T$:

1) Compute $\tilde{u} = E^{-1}(\hat{u} - \text{Sign}(E^{-1}\hat{u})\bar{u})$ where $\bar{u} = [\bar{u}_1, \bar{u}_2]^T$ and $\tilde{u} = [\tilde{u}_1 \ \tilde{u}_2]^T$. If $\tilde{u}_1 \neq 0$, $\tilde{u}_2 \neq 0$ and $\text{Sign}(E^{-1}\hat{u}) = \text{Sign}(\tilde{u})$, then a solution of the algebraic loop is found.
   Otherwise, go to step 2):

2) Set $\text{dz}_1(\hat{u}_1 - e_{12}\tilde{u}_2) = 0$ and $\tilde{u}_2 = \frac{\text{dz}_2(\hat{u}_2)}{e_{22}}$. Then if $\tilde{u}_1 = 0$, a solution is found.
   Otherwise, go to step 3):

3) Set $\text{dz}_2(\hat{u}_2 - e_{21}\tilde{u}_1) = 0$ and $\tilde{u}_1 = \frac{\text{dz}_1(\hat{u}_1)}{e_{11}}$. Then if $\tilde{u}_2 = 0$, a solution is found.

This procedure will guarantee the solution of the algebraic loop and can be extended to the case with more than two constrained signals.

IV. CONTROLLER DESIGNS, TUNING OF AW COMPENSATORS AND IMPLEMENTATION RESULTS

In this section, we first introduce the framework used for DSS robust H_∞ controller design, for both the SiM and the MuM. Then, we present the weighting functions used for the designs of H_∞ controllers and AW compensators. To make a comparison of the AW approaches and show the effect of using filters in AW tuning, we describe the real-time implementations for five cases: 1) H_∞ controller alone; 2) H_∞ controller with an IMC AW compensator; 3) H_∞ controller combined with the RAW compensator of [32], without W_{fy}; 4) H_∞ controller combined with the RAW compensator of [32], with W_{fy}; 5) H_∞ controller combined with the DRAW compensator, with W_{fy} and W_{fd}.

The control outputs were set to ± 1.5mm in the SiM and ± 750N in the MuM, in order to restrict the actuators' magnitude of saturation. These saturation bounds were used for demonstration purposes only; the actual magnitude limits of the actuators were significantly larger than these values.

The testing signal $d = [d_1, d_2]^T$ used for both the SiM and the MuM was composed of two ramped chirp sinusoidal signals, where d_2 had a 0.85s delay from d_1, representing the forward motion of the vehicle. The testing duration was 20s. An initial ramp time of 10s was used, with the magnitude increasing from 0m to 0.0025m at 10s and kept constant at 0.0025m from 10s to 20s. In order to test the performance of the DSS within a frequency range, the frequency of the testing signal swept from 15Hz to 5Hz. This testing signal was assumed to be a road disturbance, when the vehicle (1.7m in length between the front and rear wheels) was running at a speed of 2m/s.

All the real-time experiments were implemented using MATLAB 2007b® and dSPACE rti1103© at a sampling rate of 2kHz, which was far higher than the bandwidths of the closed-loop sensitivity functions of both the SiM and the MuM, when using the linear controllers described in sections IV-A and IV-B1. Note that this sampling rate is faster than the sampling rates (below 1kHz) for implementation of MPC controllers on the SiM in [18], and an even higher sampling rate could be implemented for AW compensators.

A. The framework used for the linear H_∞ controller design

For the SiM, the physical components only reside in the actuator block G_A and the interaction block G_I. For nominal controller design, suppose that the actuator block has an input multiplicative uncertainty $\tilde{G}_A = G_A(I + W_{AL}\Delta_A W_{AR})$ where $\Delta_A = \text{diag}(\delta_1, \delta_2)$ with $\|\delta_1\|_\infty \leq 1$ and $\|\delta_2\|_\infty \leq 1$; W_{AL} and W_{AR} are weighting functions with diagonal forms. G_I also contains numerical components; however, we assume that all the uncertainties in G_I are lumped into an output multiplicative uncertainty $\tilde{G}_I = (I + W_{IL}\Delta_I W_{IR})G_I$ where a 2×2 full block Δ_I satisfies $\|\Delta_I\|_\infty \leq 1$. Here, W_{IL} and W_{IR} are weighting functions with diagonal forms. Note that the uncertainty $W_{AL}\Delta_A W_{AR}$ represents the unmodelled dynamics of the actuators and measurement noises of the sensors, while the uncertainty $W_{IL}\Delta_I W_{IR}$ represents the unmodelled dynamics of the vehicle body and suspension struts. With this uncertainty representation, the DSS framework in Fig. 2 is modified to Fig. 6, where W_e is the DSS error performance weighting function. Using d and e as measured variables and $\tilde{e}$ as the performance variable, the standard $M - \Delta$ form for robust controller design can be derived [36]. Note that the multiplicative uncertainty assumption used for nominal controller design also suits the AW-design procedure, as multiplicative uncertainty is subsumed by additive uncertainty as shown in Fig. 5. For the AW compensator, this lumped additive uncertainty can be used to achieve a trade-off between robustness and performance.

For the MuM, though the physical components G_{yd1} and G_{yd2} also exist in G_d, the uncertainties from these components
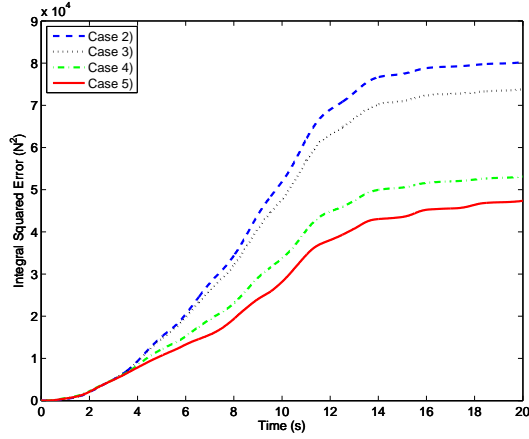
Fig. 6: Actuator multiplicative uncertainty and G_I output multiplicative uncertainty

TABLE III: The weighting functions chosen for the designs of H_∞ controllers and AW compensators in SiM and MuM

	$w(s)$	$w_e(s)$	$w_{fy}(s)$	$w_{fd}(s)$
SiM	$\frac{0.1s+10}{0.1s+100}$	$\frac{s+2000}{50s+100}$	$\frac{0.9s+72}{s+8}$	$\frac{0.8s+40}{0.8s+0.8}$
MuM	$\frac{0.25s+55}{0.5s+220}$	$\frac{(s+486)^2}{(0.5s+180)^2}$	$\frac{s+200}{s+100}$	$\frac{(0.5714s+280)^2}{(s+2.8)^2}$

are ignored since they do not affect robust stability. Hence, for the MuM, we can adopt the same configuration as the SiM in Fig. 6.

B. The choice of weighting functions for the H_∞ controller and the AW compensators

1) H_∞ controller: The weighting functions W_{AR}, W_{AL}, W_{AR}, W_{AL} all take the same diagonal form as $\mathrm{diag}(w(s), w(s))$ and the output weighting function is $W_e = \mathrm{diag}(w_e(s), w_e(s))$. In this case, the $w(s)$ and $w_e(s)$ used for SiM and MuM are shown in Table III. Note that the bandwidths of the two types of actuator dynamics, i.e. $\{G_{Ay1}, G_{Ay2}\}$ and $\{G_{Af1}, G_{Af2}\}$, are about 30rad/s and 10rad/s respectively. The weighting functions are chosen so that the magnitude of uncertainties they represent are not prominent at frequencies less than these bandwidth values, while satisfactory performances are expected by tuning higher values of $w_e(s)$ within the bandwidths.

With these weighting functions, the MATLAB routine `hinfsyn` produced two controllers with 12 states (after model reduction) for the SiM and the MuM. Both controllers resulted in closed-loop bandwidths of the SiM and MuM in the region of 15Hz.

2) AW compensators: The filters W_{fy} used in cases 4) and 5) and the filters W_{fd} used in case 5) all take diagonal forms, i.e., $W_{fy} = \mathrm{diag}(w_{fy}(s), w_{fy}(s))$ and $W_{fd}(s) = \mathrm{diag}(w_{fd}(s), w_{fd}(s))$. The weighting functions $w_{fy}(s)$ and $w_{fd}(s)$ selected for AW compensator designs for the SiM and MuM are shown in Table III. Note that these weighting functions are filters which penalize the testing signal at low frequencies. The choices of W_{fd} increase the magnitude of $\mathcal{P}_d$ at low frequencies for both the SiM and MuM. Thus, the filter W_{fd} models the testing signal acting on the DSS. Similarly, the filter W_{fy} is chosen to increase the magnitude of $\mathcal{P}_u$ at low frequencies. The weighting functions w_{fd} and w_{fy} chosen in Table III all penalize the road disturbance frequency under 15Hz.

Furthermore, in cases 4) and 5) for both the SiM and MuM, we choose $W_y = \mathrm{diag}(1, 1)$, $W_r = \mathrm{diag}(0.1, 0.1)$ and

TABLE IV: L_2 gains and fast poles for AW compensators in the SiM and MuM

	Case 4)		Case 5)	
	γ_u	Fast pole	γ_d	Fast pole
SiM	1.0970	-658.3	7.0336	-95.6
MuM	2.9007	-100.2917	55.7903	-85.4757

Fig. 7: Integral squared error comparison of 4 cases of AW compensator implementations for the SiM.

$w_d = 0.1$ in (10). This helps to achieve a trade-off between robustness and performance, and also avoids the creation of fast poles. Here, an AW compensator's *fast pole* is defined as the pole of $A_p + B_pF$ with the largest modulus.

The above choices of tuning parameters yield the γ_u, γ_d and the fast poles as shown in Table IV. Note that the fast poles resulting from case 5) are much slower than the ones from case 4), for both the SiM and MuM. This means that the hardware upper sampling rate limit is less likely to be limiting when using the DRAW approach.

The matrices E derived in case 5) are $\begin{bmatrix} 1.5776 & -0.1875 \\ 0.0068 & 1.4569 \end{bmatrix}$ and $\begin{bmatrix} 139.1651 & 7.2050 \\ 2.8278 & 24.6265 \end{bmatrix}$ for the SiM and MuM, respectively. Both matrices are invertible and the two matrices resulting from $E^{-1} \mathrm{diag}(\bar{u}, \bar{u})$ are diagonally dominant, with $\bar{u}$ as the absolute values of saturation limits in the SiM and MuM. Hence the algebraic loop problems can be resolved using the routine developed in [30].

C. Summary of DSS saturation problem solution using the AW technique

In this subsection, we summarize the main steps in the AW compensation approach for coping with the actuator saturation problem in DSS.

Procedure 3:

1) *DSS construction.* Perform the DSS synthesis according to the requirement of the dynamics testing problem (as shown in section II-B).
2) *Linear controller design.*
   2.1) Design a linear DSS controller. Tune the linear controller to achieve satisfactory robust stability and performance.
   2.2) Set hard limits on the actuator input, or on the controller output.

Fig. 8: Integral squared error comparison of 4 cases of AW compensator implementations for the MuM.

(a) No anti-windup compensation – case 1)

(b) AW for disturbance rejection – case 5)

Fig. 9: A comparison of the DSS outputs for the SiM

(a) No anti-windup compensation – case 1)
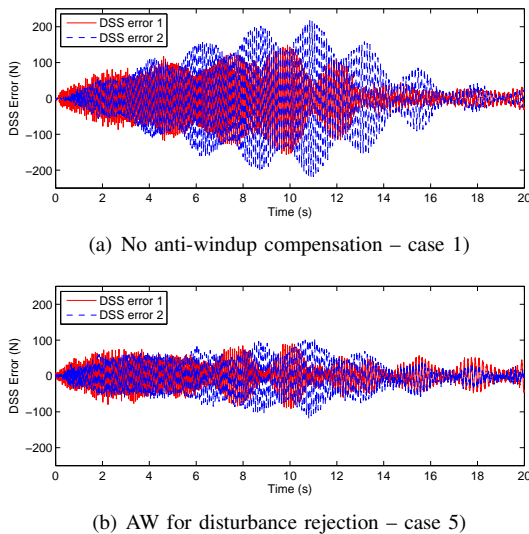

(b) AW for disturbance rejection – case 5)

Fig. 10: A comparison of the DSS outputs for the MuM

3) *Design AW compensators* (choose one of the following methods).

IMC AW

Formulate the compensator according to section III-B2.

RAW

i) Synthesize a RAW compensator using (17). Tune W_y and W_r to achieve a trade-off between robustness and performance. The fast poles should be avoided during this tuning procedure.

ii) Include a low pass filter W_{fy}, i.e. replace $\mathcal{P}_u$ by $\mathcal{P}_u W_{fy}$. The bandwidth of W_{fy} is determined by the frequency range of the testing signal. Design a RAW compensator by repetitively using (17) and running simulations to achieve the best performance through fine-tuning of W_{fy}.

DRAW

i) Synthesize a DRAW compensator according to Procedure 1. During the synthesis, tune W_y, W_r and w_d to achieve a trade-off between robustness and performance. The fast poles can be avoided by proper tuning of these parameters.

ii) Include a low pass output weight W_{fy} and a low pass disturbance filter W_{fd}, i.e. replace $\mathcal{P}_u$ by $\mathcal{P}_u W_{fy}$, $\mathcal{K}_w$ by $\mathcal{K}_w W_{fd}$ and $\mathcal{P}_w$ by $\mathcal{P}_w W_{fd}$. The bandwidth of W_{fy} and W_{fd} should match that of the testing signal. Design a DRAW compensator by repetitively using the Procedure 1 and running simulations to achieve the best performance through fine-tuning of W_{fy} and W_{fd}.

iii) Check if $E^{-1} \operatorname{diag}(\bar{u}, \bar{u})$ is diagonally dominant, with the entries of $\bar{u}$ containing the absolute values of saturation limits. If this condition is satisfied (in most cases, it is), use Procedure 2 to resolve the algebraic loop problem.

D. Implementation results

We have performed several experiments of which two sets, one for SiM and one for MuM, are presented here. The DSS errors recorded from the real-time implementation of the H_∞ controller alone (i.e. case 1)) and the H_∞ controller with the DRAW compensator (i.e. case 5)) are shown in Fig. 9 for the SiM and in Fig. 10 for the MuM. The DSS error reduction from case 1) to case 5) can be seen clearly from the figures. To better illustrate and compare the effects of different AW compensators, the integral squared DSS errors (ISE) plots of cases 2) to 5) are shown in Fig. 7. From this figure we note that W_{fy} is a key tuning parameter for the RAW performance. The RAW without an output weight W_{fy} is slightly better than the IMC AW in the MuM, but worse than the IMC AW in the SiM. However, the inclusion of W_{fy} in the RAW can achieve a better performance than the IMC AW for both the SiM and the MuM. We also note that the DRAW with a disturbance filter W_{fd}, i.e. case 5), yields the best performance.

This highlights an advantage of the DRAW-approach. Having additional degrees of freedom for design, i.e. W_{fd}, w_d, and directly addressing a disturbance rejection design problem, provides a practical advantage over the other AW-approaches.

V. Conclusion

We have designed and implemented anti-windup (AW) compensators based on linear robust H_∞ controllers for two DSS systems, based on a hydraulically-actuated quasi-motorcycle test rig. The implementation results showed the efficacy of using the AW compensators to cope with the actuator saturation problem that can be encountered in DSS systems. The DRAW compensator, designed by a novel approach incorporating disturbance rejection, was shown to achieve the best performance in terms of the reduction of substructuring errors. The tuning procedure of AW compensators and real-time implementation issues were presented and discussed.

VI. Acknowledgement

References

[1] D. P. Stoten and R. A. Hyde, "Adaptive control of dynamically substructured systems: the single-input single-output case," *Proc. IMechE Part I: Systems and Control Engineering*, vol. 220, pp. 63–79, 2006.

[2] M. S. Williams and A. Blakeborough, "Laboratory testing of substurctures under dynamic loads: an introductory review," *Phil. Trans. R. Soc. Lond. A,*, vol. 359, pp. 1651–1669, 2001.

[3] A. R. Plummer, "Model-in-the-loop testing," *Proc. IMechE Part I: Journal of Systems and Control Engineering*, vol. 220, pp. 183–199, 2006.

[4] P. G. Maghami and K. B. Lim, "Synthesis and control of flexible systems with component-level uncertainties," *Journal of Dynamic Systems, Measurement, and Control*, vol. 131, no. 5, 2009.

[5] S.-K. Lee, E. C. Park, K.-W. Min, and J.-H. Park, "Real-time substructuring technique for the shaking table test of upper substructures," *Engineering Structures*, vol. 29, pp. 2219–2232, 2007.

[6] C.-P. Lamarche, R. Tremblay, P. Léger, M. Leclerc, and O. S. Bursi, "Comparison between real-time dynamic substructuring and shake table testing techniques for nonlinear seismic applications," *Earthquake Engineering & Structural Dynamics*, vol. 39, p. 12991320, 2010.

[7] O. S. Bursi, C. Jia, V. L., S. A. Neild, and D. J. Wagg, "Rosenbrock-based algorithms and subcycling strategies for real-time nonlinear substructure testing," *Earthquake Engineering & Structural Dynamics*, 2010.

[8] J. Y. Tu, P. Y. Lin, D. P. Stoten, and G. Li, "Testing of dynamically substructured, base-isolated systems using adaptive control techniques," *Earthquake Engineering & Structural Dynamics*, vol. 39, pp. 661–681, 2010.

[9] D. P. Stoten, J. Tu, G. Li, and K. Koganezawa, "Robotic subsystem testing using an adaptively controlled dynamically substructured framework," in *9th IFAC Symposium on Robot Control*, Gifu, Japan, 2009.

[10] R. Verma, D. Del Vecchio, and H. Fathy, "Development of a scaled vehicle with longitudinal dynamics of an hmmwv for an its testbed," *Mechatronics, IEEE/ASME Transactions on*, vol. 13, no. 1, pp. 46 –57, Feb. 2008.

[11] X. Yue, D. Vilathgamuwa, and K.-J. Tseng, "Robust adaptive control of a three-axis motion simulator with state observers," *Mechatronics, IEEE/ASME Transactions on*, vol. 10, no. 4, pp. 437 – 448, 2005.

[12] M. MacDiarmid, R. Daniel, and M. Bacic, "A novel controller design methodology for uncertain non-linear hardware-in-the-loop simulators," in *46th IEEE Conference on Decision and Control*, 2007, pp. 3478–3483.

[13] M. Karpenko and N. Sepehri, "Hardware-in-the-loop simulator for research on fault tolerant control of electrohydraulic actuators in a flight control application," *Mechatronics*, vol. 19, no. 7, pp. 1067 – 1077, 2009.

[14] T. Ersal, M. Brudnak, A. Salvi, J. L. Stein, Z. Filipi, and H. K. Fathy, "Development and model-based transparency analysis of an internet-distributed hardware-in-the-loop simulation platform," *Mechatronics*, vol. 21, no. 1, pp. 22 – 29, 2011.

[15] B. Wu, Q. Wang, P. Benson Shing, and J. Ou, "Equivalent force control method for generalized real-time substructure testing with implicit integration," *Earthquake Engineering & Structural Dynamics*, vol. 36, pp. 1127–1149, 2007.

[16] P. A. Bonnet, M. S. Williams, and A. Blakeborough, "Compensation of actuator dynamics in real-time hybrid tests," *Proc. IMechE Part I: Journal of Systems and Control Engineering*, vol. 221, pp. 251–264, 2007.

[17] A. P. Darby, M. S. Williams, and A. Blakeborough, "Stability and delay compensation for real-time substructure testing," *Journal of Engineering Mechanics*, vol. 128, no. 12, pp. 1276–1284, 2002.

[18] G. Li, D. P. Stoten, and J. Tu, "Model predictive control of dynamically substructured systems with application to a servohydraulically-actuated mechanical plant," *IET Control Theory Appl.*, vol. 4, pp. 253–264, 2010.

[19] A. Zheng and M. Morari, "Anti-windup using internal model control," *International Jounal of Control*, vol. 60, pp. 1015–1024, 1994.

[20] M. V. Kothare, P. J. Campo, M. Morari, and C. N. Nett, "A unified framework for the study of anti-windup designs," *Automatica*, vol. 30, pp. 1869–1883, 1994.

[21] G. Grimm, J. Hatfield, I. Postlethwaite, A. R. Teel, M. C. Turner, and L. Zaccarian, "Antiwindup for Stable Linear Systems With Input Saturation: An LMI-Based Synthesis," *IEEE Trans. on Automatic Control*, vol. 48, no. 9, pp. 1509–1525, 2003.

[22] J. G. da Silva Jr. and S. Tarbouriech, "Anti-windup design with guaranteed regions of stability: an LMI approach," *IEEE Trans. on Automatic Control*, pp. 106–111, 2005.

[23] A. R. Teel, L. Zaccarian, and J. J. Marcinkowski, "An anti-windup strategy for active vibration isolation systems," *Control Engineering Practice*, vol. 14, pp. 17–27, 2006.

[24] G. Grimm, A. R. Teel, and L. Zaccarian, "The l_2 anti-windup problem for discrete-time linear systems: Definition and solutions," *Systems & Control Letters*, vol. 57, pp. 356–364, 2008.

[25] C. Roos and J.-M. Biannic, "A convex characterization of dynamically-constrained anti-windup controllers," *Automatica*, vol. 44, no. 9, pp. 2449 – 2452, 2008.

[26] N. Itagaki, H. Nishimura, and K. Takagi, "Two-degree-of-freedom control system design in consideration of actuator saturation," *Mechatronics, IEEE/ASME Transactions on*, vol. 13, no. 4, pp. 470 –475, aug. 2008.

[27] P. F. Weston and I. Postlethwaite, "Linear conditioning for systems containing saturating actuators," *Automatica*, vol. 36, pp. 1347–1354, 2000.

[28] G. Herrmann, M. C. Turner, I. Postlethwaite, and G. Guo, "Practical implementation of a novel anti-windup scheme in a HDD-dual-stage servo-system," *IEEE /ASME Transactions on Mechatronics*, vol. 9, no. 3, pp. 580–592, 2004.

[29] M. Walsh, M. Hayes, and J. Nelson, "Robust performance for an energy sensitive wireless body area network, an anti-windup approach," *International Journal of Control*, vol. 86, pp. 59–73, 2009.

[30] G. Li, G. Herrmann, D. P. Stoten, J. Tu, and M. C. Turner, "A disturbance rejection anti-windup framework and its application to a substructured system," in *the 47th IEEE Conference on Decision and Control*, Cancun, Mexico, 2008, pp. 3510–3515.

[31] ——, "A novel robust disturbance rejection anti-windup framework," *International Journal of Control*, vol. 84, no. 1, pp. 123–137, 2011.

[32] M. C. Turner, G. Herrmann, and I. Postlethwaite, "Incorporating robustness requirements into antiwindup design," *IEEE Transactions on Automatic Control*, vol. 52, pp. 1842–1855, 2007.

[33] ——, *Advanced Strategies in Control Systems with Input and Output Constraints*. Springer, 2006, ch. Anti-windup compensation using a decoupling architecture, pp. 121–171.

[34] D. P. Stoten, J. Tu, and G. Li, "Synthesis and control of generalised dynamically substructured systems," *Proc. IMechE Part I: Systems and Control Engineering*, vol. 223, pp. 371–392, 2009.

[35] M. C. Turner and I. Postlethwaite, "A new perspective on static and low order anti-windup synthesis," *International Journal of Control*, vol. 77, no. 1, pp. 27–44, 2004.

[36] K. Zhou, J. C. Doyle, and K. Glover, *Robust and optimal control*. Upper Saddle River, N.J.: Prentice Hall, 1996.

Guang Li Guang Li received his B.E. degree in Automatic Control and M.E. degree in Control Theory and Control Engineering, from the University of Science and Technology Beijing, in 2000 and 2003 respectively. He received his PhD degree from the Control Systems Centre, the University of Manchester in 2007. From 2007 to 2010 he worked as a postdoctoral researcher at the Advanced Control and Test Laboratory in the University of Bristol. He is now a research fellow in Exeter University. His research interests include model predictive control, robust control, nonlinear systems and control applications.

Guido Herrmann Guido Herrmann (Senior IEEE Member, CEng(IET)) received the German degree 'Diplom-Ingenieur der Elektrotechnik' (with highest honours) from the Technische Universität zu Berlin, Germany, and the Ph.D.-degree from the University of Leicester, UK, in 1997 and 2001, respectively. From 2001 to 2003, he was a Senior Research Fellow at the Data Storage Institute in Singapore. From 2003 until 2005, he was a Research Associate, Fellow and Lecturer at the University of Leicester. He joined the University of Bristol as a Lecturer in March 2007 and has been since August 2009 a Senior Lecturer. His research considers the development and application of novel robust and nonlinear control systems.

David P. Stoten David Stoten was born in Luton, UK, in 1952. He obtained a First Class Honours degree in Mechanical Engineering from the University of Salford, Manchester, in 1974. After working as a research engineer on missile flight control systems at the British Aircraft Corporation, he studied for the degree of PhD at Trinity College, the University of Cambridge. He was appointed Research Fellow of Girton College, Cambridge, in 1979, and obtained his PhD in that year. From 1979-1983 Prof Stoten was a lecturer in Mechanical Engineering at the University of Liverpool. In 1983 he became a lecturer and then reader at the University of Bristol and was promoted to Professor of Control and Dynamics in 1994. From 1998 -2004 he was Head of Department of Mechanical Engineering at Bristol. Prof Stoten was awarded a DEng from the University of Bristol in 1993 and is a Fellow of the Institution of Mechanical Engineers. Prof Stoten's main research interests include adaptive control, multivariable control, nonlinear control and the control of dynamically substructured (hybrid) systems.

Matthew Turner Matthew Turner was born in Corby, England in 1975. He received the BEng degree in Electrical and Electronic Engineering in 1996, from the University of Surrey, and the PhD in Control Engineering in 2000, from the University of Leicester. He is currently a Senior Lecturer at Leicester and serves on the editorial board of the International Journal of Control. His main research interests are centred around robust control, flight control and the control of systems containing isolated nonlinearities. He has designed and implemented robust controllers and anti-windup compensators on several industrial engineering systems, and is currently involved with research into pilot-induced-oscillations (PIOs) and helicopter vibration reduction.